Contents lists available at ScienceDirect

Inorganica Chimica Acta

journal homepage: www.elsevier.com/locate/ica



Research paper

Water wire clusters in isostructural Cu(II) and Ni(II) complexes: Synthesis, characterization, and thermal analyses



Nina Saraei^a, Oleksandr Hietsoi^a, Brian C. Frye^a, Alexander J. Gupta^b, Mark S. Mashuta^a, Gautam Gupta^b, Robert M. Buchanan^{a,*}, Craig A. Grapperhaus^{a,*}

- ^a Department of Chemistry, University of Louisville, Louisville, KY 40292, USA
- ^b Department of Chemical Engineering, University of Louisville, Louisville, KY 40292, USA

ARTICLE INFO

Keywords: Hydrogen bonding Water wires Copper Nickel 1-Methylimidazole

ABSTRACT

Hydrogen bonding (HB) interactions are well known to impact the properties of bulk water and within hydrated materials. Most notably, 1D water wires are involved in proton and water transport. Therefore, the design and synthesis of efficient proton conductors in terms of cost and performance are of great interest. In this work, isostructural Cu(II) and Ni(II) complexes based on N,N'-(ethane-1,2-diyl)bis(1-methyl-1H-imidazole-2-carboxamide) (H₂L) have been synthesized and fully characterized by single crystal X-ray diffraction, spectroscopic methods, and thermal analysis. Both complexes crystalize in the monoclinic space group P2₁/c. The asymmetric unit of 1 and 2 contain two equivalents of CuL or NiL and four molecules of water of hydration. In the solid state packing of both complexes, the extended hydrogen bonding (HB) networks form 1D coiled zig-zag chains of water along the crystallographic b-axis. For both complexes, the identical ligand framework, coordination geometries, and solid state packing result in formation of similar HB expansion motifs, which result in analogous thermal stabilities and phase transitions at elevated temperature.

1. Introduction

The design and synthesis of efficient proton conductors in terms of both cost and performance are of fundamental importance to the next generation of devices for clean energy production [1-5]. Water confined in Metal Organic Frameworks (MOFs) [6], Nafion thin films [7], and low dimensional nonporous materials provide proton carriers such as H₃O⁺ or H₃O₉⁺ associated with ligand functional groups and hydrogen bonding networks to facilitate proton conduction [6]. In biological systems, one-dimensional (1D) neutral water molecular clusters (WMCs) are thought to be involved in proton conduction [8-10]. The mechanism involved in proton transfer is thought to involve a Grotthaus process and has been studied extensively [11,12]. In addition, 1D water wires confined in nonporous materials also have been reported to display much higher proton conduction than in bulk water [13–15].

While MOFs are attractive materials for preparing proton conductors, due to their highly designable nature and diverse topological architecture [16-18], smaller and more easily accessible metal complexes that possess supramolecular properties such as extended π - π stacking, extensive hydrogen bonding and porous networks are also viable candidates for the generating solid state materials for proton

conduction [19]. The design and engineering of host environments for stabilizing various discrete water clusters are well documented [20,21]. Among the known water clusters in confined environments that demonstrate proton mobility, those with 1D coiled waters display enhanced proton conductivity in response to electrochemical potential gradients [22-24]. Herein, we report the synthesis and x-ray crystal structures of two isostructural Cu(II) and Ni(II) complexes containing the same N₄ chelate ligand. Both complexes are hydrated forming 1D coiled water chains through HB networks within crystal lattices, and have very similar solid state packing and thermal stability properties.

2. Experimental details

2.1. Materials and methods

All chemicals were obtained from commercial sources and used without further purification unless otherwise noted. Acetonitrile and methanol solvents were dried using a MBraun solvent purification system. H₂L was prepared following a previously reported procedure [25].

E-mail addresses: robert.buchanan@louisville.edu (R.M. Buchanan), craig.grapperhaus@louisville.edu (C.A. Grapperhaus).

^{*} Corresponding authors.

2.2. CuL (1)

An aqueous solution (50 mL) of $Cu(C_2H_3O_2)_2H_2O$ (0.35 g, 1.77 mmol) was added dropwise to a stirring aqueous solution (50 mL) of H_2L (0.49 g, 1.77 mmol) and sodium acetate (0.145 g, 1.77 mmol). The resulting purple solution was stirred overnight. The solvent was removed on a rotary evaporator yielding a red-purple solid which was purified on an alumina column. The pure product was isolated as a red band with MeCN/MeOH (3: 1) as the elute. X-ray quality single crystals were grown by vapour diffusion of MeCN solution into an aqueous solution of 1. Anal. Calcd. for $C_{12}H_1_4N_6O_2Cu$: C, 42.66; H, 4.18; N, 24.88. Found: C, 42.64; H, 4.23; N, 24.41. + MALDI, m/z calcd for $\{[CuL]-H\}^+$ 338.05; Found 338.05. FT-IR (ATR), cm $^{-1}$: 1450 (s), 1604 (s), 3350 (s). Electronic absorption (MeCN (22 °C)): λ_{max} (nm) (ε (cm $^{-1}$ M $^{-1}$)) 204 (2804), 258 (4728), 503 (33).

2.3. NiL (2)

An aqueous solution (50 mL) of H₂L (0.15 g, 0.543 mmol) was added dropwise to an aqueous solution (50 mL) of Ni(C₂H₃O₂)₂·4H₂O (0.135 g, 0.543 mmol) and sodium acetate (0.045 g, 0.543 mmol) while continuously stirring. The reaction was allowed to stir overnight and resulted in deep yellow solution. The solvent was removed on a rotary evaporator yielding an orange solid. The product was purified on an alumina column as an acetonitrile solution. The pure product was isolated as an orange band after elution with MeCN/MeOH (3: 1). X-ray quality single crystals were grown by vapour diffusion of MeCN solution into an aqueous solution of 2. Anal. Calcd. C₁₂H₁₄N₆O₂Ni·1.5H₂O: C, 40.04; H, 4.76; N, 23.34. Found: C, 40.43; H, 4.74; N, 23.07. + MALDI, m/z calcd for {[NiL]-H}⁺ 333.06; Found 332.99. 1 H NMR (CDCl₃): δ 3.35 (t, 4H), 4.00 (s, 6H), 6.60 (d, 2H), 6.80 (d, 2H). FT-IR (ATR), cm⁻¹: 1450 (s), 1600 (s), 3360 (s). Electronic absorption (MeCN (22 °C)): λ_{max} (nm) (ϵ (cm $^{-1}$ M $^{-1}$)) 206 (2026), 256 (3227), 336 (233), 468 (12).

2.4. Physical methods

Elemental analyses were performed by Midwest Microlab (Indianapolis, IN). IR spectra were recorded on a Thermo Nicolet Avatar 360 spectrometer with ATR attachment (4 cm⁻¹ resolution). Matrix Assisted Laser Desorption/Ionization (MALDI) was collected using a Voyager Biospectrometry DE Workstation (Applied Biosystems, Foster City, CA, USA) and the data processed using Data Explorer Software TM (Version 4.8). The MALDI matrix used for 1 and 2 was prepared by dissolving 0.18 M Paranitroaniline (PNA) in 1:1 MeOH to CHCl₃ solution. Prior to data collection, samples were dissolved in acetonitrile and 0.75 mL aliquot was spotted on the MALDI plate. Then 0.75 mL of matrix (PNA) was spotted on top of the sample by the drieddroplet method [26]. Electronic absorption spectra were recorded using an Agilent 8453 diode array spectrometer with a 1 cm path length quartz cell. NMR spectra were obtained on a Varian Inova 400 MHz spectrometer. TGA and DSC of the complexes were performed at the University of Louisville Conn Center for Renewable Energy Research. using an SDT Q600 TA analyzer. The sample pan was loaded with 15–20 mg of sample for each of three runs. Data points were collected from room temperature to 700 °C (for 1) or 1300 °C (for 2) at a ramp rate of 2 °C/min in a N2 stream with a flow rate at 100 mL/min.

2.5. Thermal analyses

TGA and DSC traces of complexes 1 and 2 are shown in Figs. S12–S15. In complexes 1 and 2, there is a clear dehydration step beginning near $40\,^{\circ}\text{C}$ with a mass loss of 10.13 and 7.96%, respectively, upon reaching $120\,^{\circ}\text{C}$. The mass change is consistent with loss of four water molecules per complex 1 and 10 water molecules per complex 11 and 12 water molecules per complex 12 from the lattice. Decomposition of the ligand frame work of 12 and 13.

occurs above 280 $^{\circ}$ C and 300 $^{\circ}$ C, respectively. Degradation is accompanied by a phase transition as indicated by the endothermic process observed by DSC [27,28]. The mass of the residue is consistent with the formation of the metal oxide.

In comparison to previously reported compounds confining 1D water chains [29], complex 1 and 2 also show the same correlation between HB motif of the hydrated crystals and temperature range of the dehydration process. Similary, the 1D coiled chains require a higher temperature to break the strong HB interactions within the channel and between the water and structural O atoms.

2.6. Crystallographic methods

An orange cube $0.25 \times 0.25 \times 0.25 \text{ mm}^3$ crystal of **2** was mounted on a glass fiber for collection of x-ray data on a Bruker SMART APEX CCD diffractometer. The SMART [30] software package (v 5.632) was used to acquire a total of 1868 thirty-second frame ω -scan exposures of data at 100 K to a $2\theta_{\rm max} = 54.50^{\circ}$ using monochromated MoKα radiation (0.71073 Å) from a sealed tube and a monocapillary. Frame data were integrated using SAINT [31] (v 6.45) to a theta max diffraction limit of 27.25° and processed to determine final unit cell parameters: a = 23.767(2) Å, b = 7.0356(6) Å, c = 18.0114(15) Å, $\beta = 105.4480(10)^{\circ}$, V = 2902.9(4) Å³, $D_{calc} = 1.656 \,\text{Mg/m}^3$, Z = 2 to produce raw hkl data that were then corrected for absorption (transmission min./max. = 0.855/0.978; $\mu = 1.365 \text{ mm}^{-1}$) using SADABS [32] (v 2.10). The structure was solved by Patterson methods in the space group $P2_1/c$ using SHELXS [33] and refined by least squares methods on F² using SHELXL [33] incorporated into the SHELXTL [34] (v 6.14) suite of programs. All non-hydrogen atoms were refined with anisotropic atomic displacement parameters. All hydrogen atoms not associated with waters of hydration were placed in their geometrically generated positions and refined as a riding model. Three waters of hydration are modeled with full occupancy oxygen atoms, O5, O6 and O7 each with two full occupancy hydrogen atoms, H5oa, H5ob, H6oa, H6ob, H7oa, H7ob. Additionally there is a fractional water with 20% occupancy each for O8, H8oa and H8ob (each refined isotropically with minimal restraints). For all 6,449 unique, reflections (R(int) 0.021) the final anisotropic full matrix least-squares refinement on F² for 432 variables converged at R1 = 0.034 and wR2 = 0.071 with a GOF of 1.03.

X-ray structural analysis for 1 was performed on a $0.213 \times 0.174 \times 0.124 \,\mathrm{mm}^3$ red block using an identical data acquisition strategy described above for 2 at 100 K to a $2\theta_{\text{max}} = 51.80^{\circ}$ and processed to a theta max diffraction limit of 25.90°. Complex 1 crystallizes in the space group $P2_1/c$ with unit cell parameters: $a = 24.117(5) \text{ Å}, b = 7.0125(15) \text{ Å}, c = 18.203(4) \text{ Å}, \beta = 105.597(3)^{\circ},$ $V = 2965.1(11) \text{ Å}^3$, Z = 2 and $D_{calc} = 1.655 \text{ Mg/m}^3$. The 6272 raw independent data were corrected for absorption (transmission min./ max. = 0.747/0.840; $\mu = 1.502 \,\text{mm}^{-1}$) using SADABS. The structure was solved by Patterson methods using SHELXTL [34]. All non-hydrogen atoms were refined with anisotropic atomic displacement parameters. Hydrogen atoms were refined exactly as described above for 2. Three waters of hydration are modeled with full occupancy oxygen atoms, O5, O6 and O7 each with two full occupancy hydrogen atoms, H5oa, H5ob, H6oa, H6ob, H7oa, H7ob. Additionally there is a one-half water molecule with 50% occupancy each for O8, H8oa and H8ob (each refined isotropically with minimal restraints). For all 6272 unique reflections (R(int) 0.029) the final anisotropic full matrix leastsquares refinement on F^2 for 451 variables converged at R1 = 0.043and wR2 = 0.104 with a GOF of 1.09.

2.7. Electrochemical impedance spectroscopy

Electrochemical impedance spectroscopy (EIS) was carried out on a single crystal of **2** by connecting two contacts to the same crystal face and then running these leads to the working/working sense and

counter/reference electrode ports respectively of a Metrohm Autolab PGSTAT128N potentiostat/galvanostat operating in potentiostatic mode. The crystal and contacts were enclosed in a glass chamber, and the pressure was pumped down to 17 Torr (water vapor); impedance studies were conducted at ambient temperature ($\sim\!25\,^{\circ}\text{C}$). A direct bias of 0 V was applied across 2, and an alternating bias of \pm 10 mV was applied, starting at a frequency of 100 kHz and ending at 0.1 Hz, taking ten data points per decade of frequency. At each data point, real, imaginary, and combined impedances as well as the phase angle between applied voltage and current response were acquired. Raw impedance data were imported into Zview software where the data points were fitted to an equivalent circuit model using the method of least squares.

3. Results and discussion

3.1. Synthesis and characterization

Two isostructural complexes, CuL (1) and NiL (2) were synthesized through the reaction between N, \acute{N} -(ethane-1,2-diyl)bis(1-methyl-1H-imidazole-2-carboxamide) (H₂L) and acetate salts of Cu(II) and Ni(II), respectively (Scheme 1).

The UV–Vis spectra of 1 and 2 were recorded in acetonitrile (Figs. S3 and S4). The electronic spectrum of the square planar complex 1 displays charge transfer bands at 204 and 258 nm and d-d transitions at 503 nm. Similarly, complex 2 shows absorbances at 206, 256 and 336 nm associated with charge transfer bands and 468 nm for d-d transitions.

The FT-IR spectra of 1 and 2 were collected on crystalline samples by attenuated total reflectance (ATR correction) (Figs. S5–S7). The spectra of 1 and 2 show distinct C–N and C=O stretches associated with the carboxamide moiety that are shifted relative to $\rm H_2L$ due to deprotonation. The $\rm v_{C=O}$ stretches in 1 and 2 are 1604 and 1600 cm⁻¹, respectively and are shifted from 1635 cm⁻¹ in $\rm H_2L$. Additionally, the $\rm v_{C-N}$ stretches in 1 and 2 are identical with a value of 1450 cm⁻¹ that is shifted from 1527 cm⁻¹ in $\rm H_2L$.

3.2. Crystallographic studies

Crystal data and structure refinement details for 1 and 2 are listed in Table 1. Crystals of both complexes contain water of hydration through HB interactions with the metal-ligand complex. A summary of bond distances and angles for 1 and 2 are listed in Table 2 with a summary of HB metric parameters presented in Table 3.

Complex 1 crystallizes as a red cube and is isostructural with the orange cube crystals of complex 2. Both complexes are in the monoclinic space group $P2_1/c$. The asymmetric unit of 1 contains two equivalents of CuL and four molecules of water of hydration (Fig. 1). Three waters of hydration are modeled with full occupancy oxygen (O5, O6, and O7) and hydrogen atoms. Additionally, the fourth water molecule is modeled with half occupancy oxygen (O8) and hydrogen atoms. The Cu is coordinated in a pseudo-square planar environment.

The molecules of water of hydration in 1 participates in multiple HB interactions. The O7 water molecule bridges two symmetrically

Table 1
Crystal data and structure refinement for 1 and 2.

Identification code	1	2
Empirical formula	C ₄₈ H ₅₆ Cu ₄ N ₂₄ O ₈ ·7H ₂ O	C ₄₈ H ₅₆ Ni ₄ N ₂₄ O ₈ ·6.4H ₂ O
Formula weight	1477.44	1447.31
Temperature (K)	100(2)	100(2)
Wavelength (Å)	0.71073	0.71073
Crystal system	Monoclinic	Monoclinic
Space group	$P2_1/c$	$P2_1/c$
Unit cell dimensions		
a (Å)	24.117(5)	23.767(2)
b (Å)	7.0125(15)	7.0356(6)
c (Å)	18.203(4)	18.0114(15)
α (deg)	90.00	90.00
β (deg)	105.597(3)	105.4480(10)
γ (deg)	90.00	90.00
V (Å ³)	2965.1(11)	2902.93
Z	2	2
$d_{\rm calcd} ({\rm Mg/m}^3)$	1.657	1.656
Abs coeff (mm ⁻¹)	1.502	1.365
F(000)	1524	1504
Cryst. color and habit	Red block	Orange block
Cryst. size (mm ³)	$0.21 \times 0.17 \times 0.12$	$0.24 \times 0.17 \times 0.10$
θ range for data coll.	3.03–26.75	3.12–27.25
Index ranges	$-30 \le h \le 30$	$-30 \le h \le 29$
	$-8 \le k \le 8$	$-8 \le k \le 9$
	$-23 \le l \le 23$	$-23 \le l \le 22$
Reflns collected	24,001	23,403
Independent reflections	6272 [R(int) = 0.0295]	6449 [R(int) = 0.0211]
Completeness to θ_{max}	99.6%	99.7%
Absorption correction	multi-scan	multi-scan
Max, min	0.975 and 0.815	0.978 and 0.855
transmission		
Refinement method	Full-matrix-least-squares on F ²	Full-matrix-least-squares or F ²
Data/restrains/	6272/8/451	6449/3/432
params		
Goodness of fit on F^2	1.087	1.031
Final R indices	R1 = 0.0405	R1 = 0.0282
$[I > 2\sigma(I)]^{a,b}$	wR2 = 0.1031	wR2 = 0.0683
R indices (all data) ^{a,b}	R1 = 0.0433	R1 = 0.0337
	wR2 = 0.1048	wR2 = 0.0709
Largest diff. peak and hole (e··· \mathring{A}^{-3})	0.625 and -0.357	0.450 and -0.252

[a] R1 = $\Sigma ||F_o| - |F_c||/\Sigma |F_o|$. [b] wR2 = $\{\Sigma [w(F_o^2 - F_c^2)^2]/\Sigma [w(F_o^2)^2]\}^{-1/2}$, where $w = q/\sigma^2(F_o^2) + (qp)^2 + \text{bp. GOF} = S = \{\Sigma [w(F_o^2 - F_c^2)^2]/(n-p)\}^{1/2}$, where n is the number of reflections and p is the number of parameters refined.

equivalent metal complexes through HB interactions of H7oa and H7ob with the carboxamide oxygen atoms $O2^{ii}$ (-x+1, -y+1, -z+1) and O2 (x, y, z), respectively. These two H-bonds are slightly bent with an O7-H7oa···O2 ii (-x+1, -y+1, -z+1) angle of $167(4)^\circ$ and O7-H7ob···O2 angle of $164(5)^\circ$. The donor-acceptor (D···A) and hydrogen-acceptor (H···A) distances of O7-H7oa···O2 are 2.738(3) Å and 1.91(2) Å, respectively and are consistent with a strong interaction. Similarly, (D···A) and (H···A) distances of O7-H7ob···O2 are 2.814(3) Å and 1.99(2) Å, respectively and indicate characteristics of a strong interaction.

Both O5 and O6 are involved in 3 HB interactions each and

OEt Toluene
$$H_2L$$
 $M(CH_3COO)_2$ H_2O, CH_3COONa $M = Cu^{2+}(1), Ni^{2+}(2)$

Scheme 1. Synthetic pathway for complexes 1 and 2.

Table 2
Selected bond distances (Å) and bond angles (°) for 1 and 2.

Bonds	1	2
Cu1-N3	1.913(2)	
Cu1-N4	1.934(2)	
Cu1-N1	1.957(2)	
Cu1-N5	1.970(2)	
Cu2-N10	1.919(2)	
Cu2-N9	1.922(2)	
Cu2-N7	1.974(2)	
Cu2-N11	1.984(2)	
Ni1-N3		1.8305(14)
Ni1-N4		1.8469(14)
Ni1-N1		1.8838(14)
Ni1-N5		1.8971(14)
Ni2-N10		1.8381(15)
Ni2-N9		1.8404(15)
Ni2-N7		1.9001(14)
Ni2-N11		1.9013(15)
Angles		
N3-Cu1-N4	82.90(10)	
N3-Cu1-N1	84.08(10)	
N4-Cu1-N1	166.97(9)	
N3-Cu1-N5	166.44(10)	
N4-Cu1-N5	83.63(9)	
N1-Cu1-N5	109.39(9)	
N10-Cu2-N9	82.87(10)	
N10-Cu2-N7	166.47(10)	
N9-Cu2-N7	83.85(10)	
N10-Cu2-N11	83.22(10)	
N9-Cu2-N11	166.08(10)	
N7-Cu2-N11	110.02(10)	
N3-Ni1-N4		84.75(6)
N3-Ni1-N1		85.13(6)
N4-Ni1-N1		169.81(6)
N3-Ni1-N5		169.81(6)
N4-Ni1-N5		85.06(6)
N1-Ni1-N5		105.06(6)
N10-Ni2-N9		84.44(6)
N10-Ni2-N7		169.41(7)
N9-Ni2-N7		84.97(6)
N10-Ni2-N11		84.77(7)
N9-Ni2-N11		169.18(6)
N7-Ni2-N11		105.81(6)

Table 3
Selected HB metrics for 1 and 2.

D-H···A	H…A (Å)	D···A (Å)	D-HA (°)
1			
O5-H5obO(3)i	1.94(2)	2.777(3)	169(4)
O5-H5oaO(6)	1.843(19)	2.698(3)	178(4)
O6-H6ob···O(5)i	1.914(19)	2.769(3)	177(4)
O6-H6oaO(1)	1.89(2)	2.742(3)	170(4)
O7-H7obO(2)	1.99(2)	2.814(3)	164(5)
O7-H7oa···O(2)ii	1.91(2)	2.738(3)	167(4)
O8-H8oa···O(4)	1.98(3)	2.837(6)	168(9)
Symmetry codes: $i =$	-x, $y + 1/2$, $-z +$	1/2; ii = $-x + 1, -$	y + 1, -z + 1
2			
O5-H5oa···O(6)	1.88(3)	2.691(2)	175(3)
O5-H5obO(3)i	2.00(3)	2.7718(19)	172(2)
O6-H6obO(1) ⁱⁱ	1.93(3)	2.7256(19)	174(3)
O6-H6oa···O(5) ⁱⁱⁱ	1.937(17)	2.766(2)	174(2)
O7-H7oa···O(2)iv	1.94	2.7538(18)	169.0
O7-H7ob···O(2)v	2.04	2.8454(19)	173.0

Symmetry codes: i = -x, -y + 1, -z + 1; ii = x, y, z + 1; iii = -x, y + 1/2, -z + 3/2; iv = x, -y + 3/2, z + 1/2; v = -x + 1, y + 1/2, -z + 1/2.

contribute both as HB donors and acceptors. Each serves as an HB donor to a carboxamido O of the ligand backbone. O5 exists in a nearly linear HBs with $O3^i$ (-x, y + 1/2, -z + 1/2) with a O5-H5ob···O3ⁱ angles of 169(4)° and (D···A) and (H...A) distances of 2.777(3) Å and 1.94(2) Å, repectively.

A similar HB interaction is observed between O6 and O1 with a O6-H6oa···O1 angle of $170(4)^\circ$ and $(D\cdots A)$ and $(H\cdots A)$ distances of 2.742(3) Å and 1.89(2) Å. In addition, O5 and O6 water molecules are linked through a pair of strong HB interactions in which each serves as a donor and acceptor. As a donor, O5 exists in nearly linear HBs with O6 with a O5-H5oa···O6 angle $178(4)^\circ$ and $(D\cdots A)$ and $(H\cdots A)$ distances of 2.698(3) Å and 1.843(19) Å, repectively.

The O6 water molecule serves as an donor with a nearly linear HB to $O5^i$ (-x, y + 1/2, -z + 1/2) with a O6-H6ob···O5ⁱ angle of 177(4)° and related (D···A) and (H···A) distances of 2.769(3) Å and 1.914(19) Å.

The water molecule O8 participates in only one HB, with the caboxamido oxygen O4. The absence of an extended HB network for O8 is consistent with its lower occupancy (50%) in the crystal lattice. The O8-H8oa···O4 angle is slightly bent, 168(9)°. The (D···A) and (H···A) distances of 2.837(6) Å and 1.98(3) Å, respectively, are associated with a strong HB interaction.

The extended HB networks in 1 can be described as 1D coiled zigzag chains of water along the b direction that are anchored to stacked metal complexes (Figs. 2 and S18). Using the graph set notation [36], the 1D water coiled chain is described as $C_2^2(4)$ (blue dotted line). The $C_2^2(4)$ chains are held between carboxamide oxygens (O1 and O3) by two $D_2^2(5)$ motifs (red dotted line). Further, carboxamide oxygens O2 also participate in $R_4^2(8)$ motif (green dotted line) which result in formation of isolated water pools. These pools are orienting the complexes into a twisted AAAA stacking arrangement.

The asymmetric unit of $\mathbf{2}$ contains two equivalents of NiL and four waters of hydration (Fig. 3). Three waters of hydration are modeled with full occupancy oxygen atoms, O5, O6, and O7. The fourth water molecule, O8, is modeled with 20% occupancy. The Ni center of $\mathbf{2}$ similar to $\mathbf{1}$ sits in the same N_4 donor environment arranged in pseudosquare planes. The four water molecules of hydration in $\mathbf{2}$ are involved in HB interactions similar to $\mathbf{1}$ (Fig. 4, Table 3).

Similar to 1, the extended HB networks in 2 consists of 1D coiled zig-zag chains of water along the b direction that are anchored to stacked metal complexes in a twisted AAAA arrangement (Fig. 4). The $C_2^2(4)$ chains (blue dotted line) are also held between carboxamide oxygens (O1 and O3) by two $D_2^2(5)$ motifs (red dotted line). Further, carboxamide oxygens O2 also participate in $R_4^2(8)$ motif (green dotted line) which result in formation of isolated water pools as in 1.

The impedance of crystal 2 was evaluated using electrochemical impedance spectroscopy (EIS). Two peaks (time constants) were observed in the plot of phase angle vs. frequency (Bode representation, Fig. S16A, red trace), indicating the presence of two interfacial electrochemical processes in 2 under the experimental conditions studied here. The presence of two time constants is confirmed by the Nyquist representation (Fig. S16B) which shows two semicircles. A single time constant is typically modelled with a single RC element (resistor and constant phase element in parallel) [37]. Therefore, in this case, we modelled the system [38] with two RC elements to account for each time constant and an additional resistive element, R1, which accounts for the equivalent series resistance of the system, including wires and contacts (R- (CPE1-R1)-(CPE-2-R2)) (Fig. S17). The phase peak at high frequency in Fig. S16A, the left-hand semicircle in Fig. S16B, and the R2-CPE1 element in Fig. S17 correspond to time constant 1. Conversely, the phase peak at lower frequency in Fig. S16A, the right-hand incomplete semicircle in Fig. S16B, and the R3-CPE2 element in Fig. S17 correspond to time constant 2. Parameters obtained by fitting the impedance data to the equivalent circuit model are presented in Table S2.

The total impedance, Z, is a combination of real (Z') and imaginary (Z") contributions to impedance [39]. At high frequency ($\sim 100 \ kHz$), the real (resistive) component of impedance represents the approximate system resistance. For 2, the system resistance (R $_{ES}$, Table S2) is approximately 360 Ω . The imaginary component, Z", constitutes both capacitive and inductive contributions to the overall impedance. In this case, both resistive and capacitive elements contribute to the system impedance. The capacitances for time constants 1 and 2 were

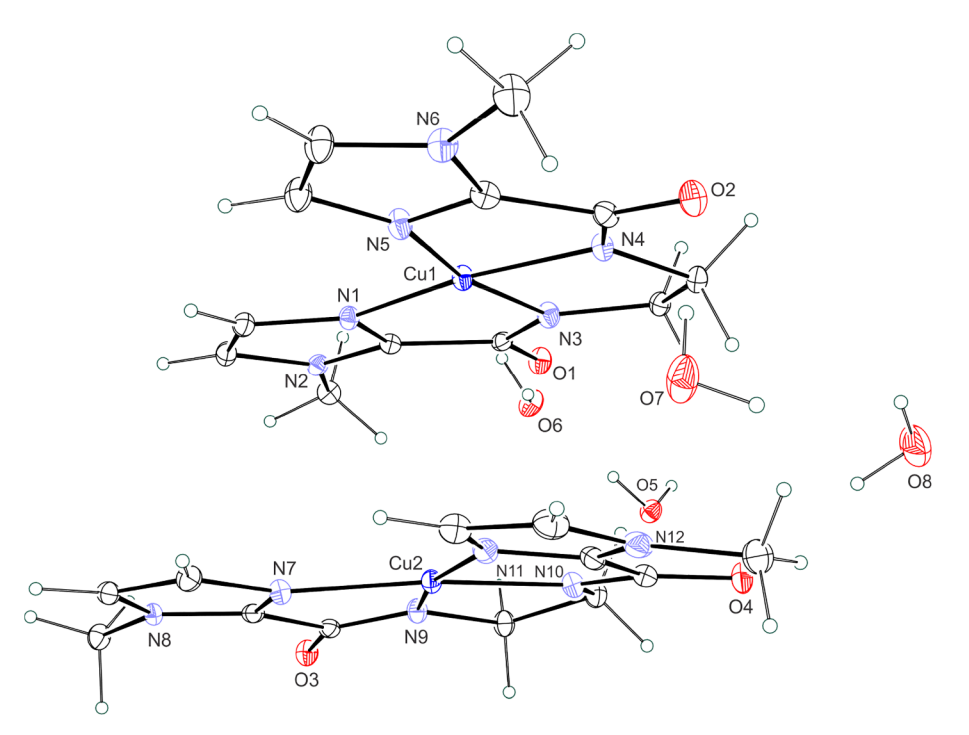


Fig. 1. ORTEP [35] representation of the asymmetric unit of CuL (1) with thermal ellipsoids shown at the 50% probability level.

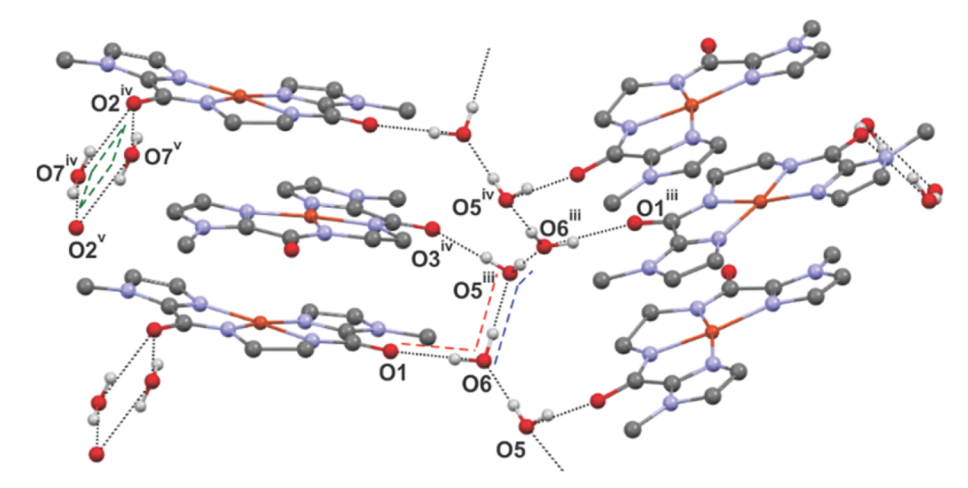


Fig. 2. The 1D HB wire of water in complex **1.** HB interactions are denoted by black dashed lines. The graph sets are noted by dotted colored lines as follows: $C_2^2(4)$ (blue); $D_2^2(5)$ (red); $R_4^2(8)$ (green). Atoms generated by symmetry are marked as follows: iii = $(-x, \frac{1}{2} + y, \frac{1}{2} - z)$, iv = (x, 1 + y, z), v = (1 - x, 2 - y, 1 - z). (For interpretation of the references to color in this figure legend, the reader is referred to the web version of this article.)

determined to be approximately 0.1 nF and 1 µF respectively.

The presence of two time constants in 2 suggests the presence of two different types of domains within the structure of the material. Introducing additional water as a dielectric into a capacitive system decreases the electric field strength, which decreases the voltage and in turn increases the capacitance. Because the capacitance of time constant 2 is several orders of magnitude higher than that of time constant 1, we postulate that the domain corresponding to time constant 2 is significantly more water-permeable and amenable to charge conduction. This wet domain (time constant 2) could be associated with water wire clusters within 2, while the dry domain corresponding to time constant 1 could be associated with charge transfer through desiccated regions of 2 which are water-deficient.

4. Conclusions

The HB motifs in isostructural planar Cu(II) (1) and Ni(II) (2) complexes are identical due to similar crystal packing of the host

molecules (Figs. 2 and 4). The interlayer HB interactions in 1 and 2 result in a twisted AAAA stacking arrangement, which positions the carbonyl O atoms to be in interaction with water molecules confined in coiled 1D chains. The thermal properties of the hydrated structures correlate with the identical HB motifs. The HB motifs facilitate orientation of the metal stacks to support propagation of the charge carriers. Based on EIS there are two types of domains present in the structure which correlate with two distinct charge transfer pathways. From a design standpoint the N,N'-(ethane-1,2-diyl)bis(1-methyl-1Himidazole-2-carboxamide) ligand can be modified by varying the ligand backbone and the steric bulk around the carboxamido-O can be used to modulate the spacing and orientation between complexes in the stack which can accordingly control the HB motifs, dehydration temperatures, and tune the conductivity. The combination of the last effects can be used to design materials that undergo structural changes upon dehydration with quantifiable effects on the charge transfer properties of the materials. Studies of this type are underway.

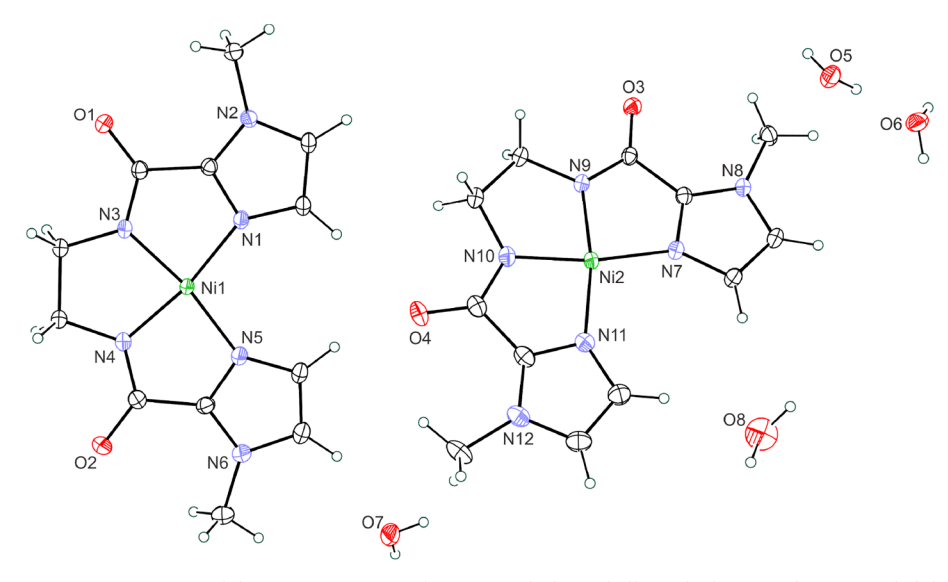


Fig. 3. ORTEP representation of the asymmetric unit of NiL (2) with thermal ellipsoids shown at the 50% probability level.

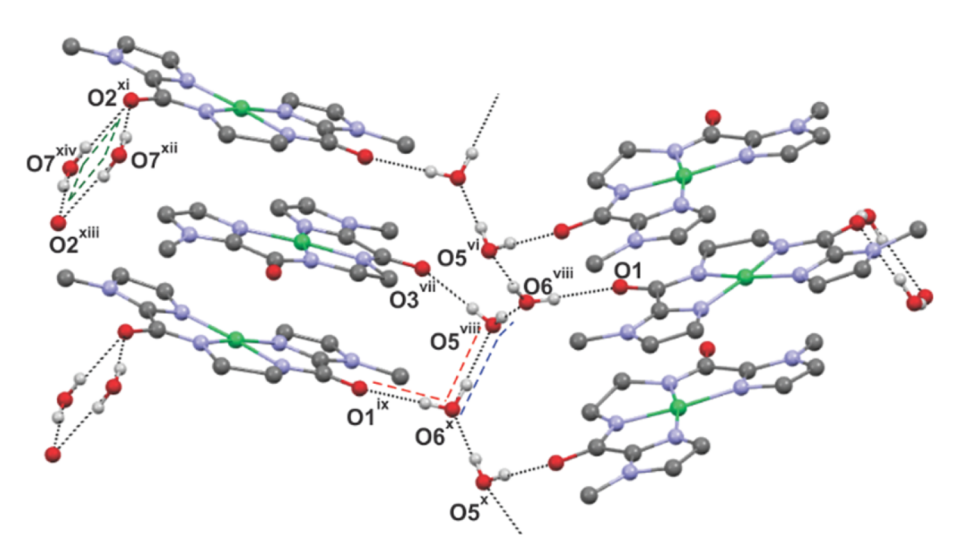


Fig. 4. The 1D HB wire of water in complex **2.** HB interactions are denoted by black dashed lines. The graph sets are noted by dotted colored lines as follows: $C_2^2(4)$ (blue); $D_2^2(5)$ (red); $R_4^2(8)$ (green). Atoms generated by symmetry are marked as follows: $vi = (-x, \ \frac{1}{2} + y, \ \frac{1}{2} - z)$, $vii = (-x, \ 1 - y, -z)$, viii = (x, y, -1 + z), $ix = (-x, -\frac{1}{2} + y, -\frac{1}{2} - z)$, $x = (-x, -\frac{1}{2} + y, -\frac{1}{2} - z)$, xii = (-x, 2 - y, -z), $xiii = (-1 + x, 1.5 - y, -\frac{1}{2} + z)$, xiv = (-1 + x, y, -1 + z). (For interpretation of the references to color in this figure legend, the reader is referred to the web version of this article.)

Acknowledgments

This research was supported by the United States National Science Foundation CHE-1665136 and CHE-1800245. MSM thanks the Department of Energy (DEFG02-08CH11538) and the Kentucky Research Challenge Trust Fund for upgrade of our X-ray facilities.

Appendix A. Supplementary data

Supplementary data to this article can be found online at https://doi.org/10.1016/j.ica.2019.04.011.

References

- [1] S. Hossain, A.M. Abdalla, S.N.B. Jamain, J.H. Zaini, A.K. Azad, Renew. Sust. Energ. Rev. 79 (2017) 750–764.
- [2] P. Ramaswamy, N.E. Wong, G.K.H. Shimizu, Chem. Soc. Rev. 43 (2014) 5913–5932.
- [3] M. Yoon, K. Suh, S. Natarajan, K. Kim, Angew. Chem. Int. Ed. 52 (2013) 2688–2700.
- [4] T. Yamada, K. Otsubo, R. Makiura, H. Kitagawa, Chem. Soc. Rev. 42 (2013) 6655–6669.
- [5] S. Shalini, V.M. Dhavale, K.M. Eldho, S. Kurungot, T.G. Ajithkumar, R. Vaidhyanathan, Sci. Rep. 6 (2016) 32489.
- [6] S.C. Sahoo, T. Kundu, R. Banerjee, J. Am. Chem. Soc. 133 (2011) 17950–17958.
- [7] K.A. Mauritz, R.B. Moore, Chem. Rev. 104 (2004) 4535–4585.
- [8] M. Tadokoro, Y. Ohhata, Y. Shimazaki, S. Ishimaru, Y. Nagao, T. Sugaya, K. Isoda, Y. Suzuki, H. Kitagawa, H. Matsui, Chem. Eur. J. 20 (2014) 13698–13709.

- [9] M. Barboiu, A. Gilles, Acc. Chem. Res. 46 (2013) 2814-2823.
- Y. Miao, R. Fu, H. Zhou, T.A. Cross, Structure 23 (2015) 2300–2308.
 L.R. Phillips, C.D. Cole, R.J. Hendershot, M. Cotten, T.A. Cross, D.D. Bus.
- [11] L.R. Phillips, C.D. Cole, R.J. Hendershot, M. Cotten, T.A. Cross, D.D. Busath, Biophys. J. 77 (1999) 2492–2501.
- [12] E.R. Decker, D.G. Levitt, Biophys. J. 53 (1988) 25-32.
- [13] H. Dong, G. Fiorin, W.F. Degrado, M.L. Klein, J. Phys. Chem. B. 118 (2014) 12644–12651.
- [14] M. Zhu, L. Han, Q. Wang, M. Wei, T. Su, C. Sun, X. Wang, Z. Su, Inorg. Chem. Commun. 96 (2018) 153–158.
- [15] K. Li, J. Gu, Y. Wang, M. Wei, B. Liu, S. Liang, H. Zang, Y. Li, H. Tan, Y. Wang, W. Guan, Z. Su, Solid State Ionics 321 (2018) 43–47.
- [16] S.S. Park, A.J. Rieth, C.H. Hendon, M. Dinca, J. Am. Chem. Soc. 140 (2018) 2016–2019.
- [17] S.K. Konavarapu, A. Goswami, A.G. Kumar, S. Banerjee, K. Biradha, Inorg. Chem. Front. 6 (2019) 184–191.
- [18] P.G.M. Mileo, K. Adil, L. Davis, A. Cadiau, Y. Belmabkhout, H. Aggarwal, G. Maurin, M. Eddaoudi, S. Devautour-Vinot, J. Am. Chem. Soc. 140 (2018) 13156–13160.
- [19] L.R. MacGillivray, Metal Organic Frameworks, Design and Application, Wiley, Hoboken, 2010.
- [20] L. Infantes, S. Motherwell, CrystEngComm 4 (2002) 454-461.
- [21] L. Infantes, J. Chisholm, S. Motherwell, CrystEngComm 5 (2003) 480-486.
- [22] J. Ponniah, S.K. Barik, R. Borthakur, A. Thakur, B. Garai, S. Jana, S. Ghosh, RSC. Adv. 5 (2015) 15690–15694.
- 23] Y. Matsuki, M. Iwamoto, K. Mita, K. Shigemi, S. Matsunaga, S. Oiki, J. Am. Chem. Soc. 138 (2016) 4168–4177.
- [24] A.R. Liboff, C. Poggi, P. Pratesi, Electromagn Biol. Med. 36 (2017) 265–269.
- [25] C. Bohlender, M. Wolfram, H. Goerls, W. Imhof, R. Menzel, A. Baumgaertel, U.S. Schubert, U. Mueller, M. Frigge, M. Schnabelrauch, R. Wyrwa, A. Schiller, J. Mater. Chem. 22 (2012) 8785–8792.
- [26] M. Karas, F. Hillenkamp, Anal. Chem. 60 (1988) 2299-2301.
- [27] Y. Roos, M. Karel, Biotechnol. Prog. 6 (1990) 159–163.

- [28] L. Yu, Adv. Drug Delivery Rev. 48 (2001) 27-42.
- [29] N. Saraei, O. Hietsoi, C.S. Mullins, A.J. Gupta, B.C. Frye, M.S. Mashuta, R.M. Buchanan, C.A. Grapperhaus, CrystEngComm 20 (2018) 7071–7081.
- [30] SMART (v 5.632), Bruker AXS Inc., Madison, WI, (2005).
- [31] SAINT (v 6.45), Bruker AXS Inc., Madison, WI, (2003).
 [32] G. M. Sheldrick, SADBS (v 2.10), University of Göttingen, Göttingen, Germany,
- [33] G.M. Sheldrick, Acta Crystallogr. Sect. A Found. Crystallogr. 64 (2008) 112–122.
 [34] G. M. Sheldrick, SHELXTL (v 6.14), Bruker AXS Inc., Madison, WI, (2004).
- [35] L.J. Farrugia, J. Appl. Crystallogr. 45 (2012) 849-854.
- [36] M.C. Etter, J.C. MacDonald, J. Bernstein, Acta Crystallogr. Sect. B Struct. Sci. 46 (1990) 256-262.
- [37] J. Huang, Z. Li, B.Y. Liaw, J. Zhang, J. Power Sour. 309 (2016) 82-98.
- [38] D. Johnson, ZView: A software program for IES analysis, Version 2.8, Scribner Associates. Inc., Southern Pines, NC (2002), 200.
- [39] J.R. Macdonald, E. Barsoukov, Impedance spectroscopy: theory, experiment, and applications, History 1 (2005) 1-13.